Unmanned Aircraft Systems Detect and Avoid Sensor Hybrid Estimation Error Analysis

Adriano Canolla,* Michael B. Jamoom,† and Boris Pervan‡

Illinois Institute of Technology, Chicago, IL, 60616, USA

This research aims at improving the methods to evaluate Detect and Avoid (DAA) sensors of Unmanned Aircraft Systems (UAS) through multiple model estimation to track maneuvering intruders. This paper builds on previous work that used predefined aircraft encounter trajectories. An established encounter model generates the intruder trajectories while multiple models are introduced to improve intruder dynamics estimation. The efficiency of the trajectory estimation has direct implication on the intruder's estimation of the closest point of approach to the own aircraft. The methods described in this research can aid a certification authority in determining if a DAA system is sufficient for UAS integration into the National Airspace System.

I. Introduction

This research describes new methods to apply safety standards in Detect and Avoid (DAA) functions for Unmanned Aircraft Systems (UAS) using target tracking and encounter models. With the expanding range of applications for UAS operations, the United States Congress mandated the Federal Aviation Administration (FAA), through the FAA Modernization and Reform Act of 2012, to develop necessary requirements for integration of UAS into the National Airspace System[REF]. One of the challenges for the FAA to meet this mandate is to ensure that safety targets are met. While a manned aircraft's pilot relies on human vision to see and avoid non-cooperative intruders (those not employing a transponder or Automatic Dependent Surveillance-Broadcast, ADS-B), an unmanned aircraft system requires a DAA system to provide self-separation between the own unmanned aircraft and the intruder aircraft. Previous work used predefined linear encounter trajectories (either with constant velocity or linear acceleration) for the sensor uncertainty analysis, focusing on potential borderline cases as a test for the methodology[REF]. In this work, an established encounter model generates the intruder trajectories. This better accounts for the likelihood of different types of encounters, to include potential worst case intruder trajectories. In addition, where previous research implemented a single Kalman filter to estimate the relative intruder aircraft dynamics[REF], the methods in this research aim to improve the intruder dynamics estimation using multiple models to track the maneuvering target. This paper serves as a continuation effort to evaluate the Multiple Model Adaptive Estimation (MMAE) tracking concept applied to realistic trajectories on the UAS DAA capabilities.[1]

I.A. Well Clear / CPA

Since a UAS will not have a pilot on board, it will have to replicate the pilot vision through appropriate sensors. DAA sensors include radar, Laser/Light Detection and Ranging (LIDAR), Electro-Optical (EO), acoustic, and Infrared (IR).[2,3] The self-separation (SS) concept had never been fully defined, despite being a widely recognized term by the FAA and International Civil Aviation Organization (ICAO).[4] The Radio Technical Commission for Aeronautics (RTCA) Special Committee-228 (SC-228), in their draft of the Detect

*PhD Candidate, Department of Mechanical, Materials and Aerospace Engineering, 10 W 32nd Street, Room 243, Student Member AIAA.

†Senior Research Associate, Department of Mechanical, Materials and Aerospace Engineering, 10 W 32nd Street, Room 243, Member AIAA.

‡Professor, Department of Mechanical, Materials and Aerospace Engineering, 10 W 32nd Street, Room 243, Associate Fellow AIAA.

and Avoid (DAA) Minimum Operational Performance Standards (MOPS), defined the Well Clear Threshold the (WCT) as the time τ to horizontal closest point of approach (CPA), of 35 seconds, a horizontal miss distance (MD) of 4000 ft, and a vertical miss distance of 450 ft.[5]

When an intruder cannot remain well clear, a collision avoidance maneuver is required to avoid a near mid-air collision (NMAC). NMAC limits are defined as 500ft laterally and 100ft vertically from the own aircraft[6] and are shown, along with the WCT and CPA, in Figure 1.

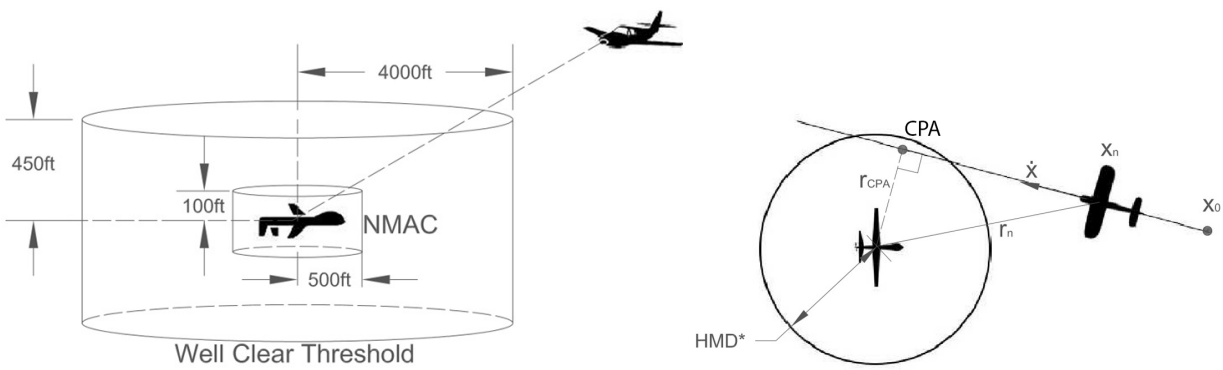

Figure 1: Well Clear Threshold, CPA, and NMAC

Our work will be focused on the WCT and Self-Separation, although the same methodology would be applied in the same way for the other thresholds.

I.B. Target Tracking

For target tracking of maneuvering targets, two main difficulties arise, one being the measurement uncertainty (due to sensor noise) and the other being poorly-known or significant changes in target behavior[REF]. The standard Kalman filter (KF) with a single motion model is limited in performance for such problems due to ineffective responses to dynamics changes as the target maneuvers. In these cases, state estimation can be modeled as a Multiple Model Adaptive Estimation (MMAE) to account for different target behavior[REF].

I.B.1. Multiple Model Adaptive Estimation

In this estimation, it is assumed that the current model is one from a discrete set of r models, combining state hypotheses from multiple filters. These filters run in parallel to estimate the states of targets with changing dynamics. We assume that for each model we have some prior probability. Also, the probabilities of switching from model i to model j in the next time step are assumed to be known. This can be seen as a transition probability matrix of a first order Markov chain characterizing the mode transitions. These systems are called hybrid since they have both continuous (noise) and discrete (mode or model) uncertainties.

I.B.2. IMM Algorithm

The optimal approach to filtering the states of a multiple model system requires running optimal filters for every possible model sequence. That is, for r models, r^n optimal filters must be run to process the measurement at time step n. In this way, an approximation is needed in practical applications of multiple model systems. Among some of the practical algorithms for the MMAE is the Interacting Multiple Model (IMM), whose model changes according to a finite-state, discrete-time Markov chain [REF].

The IMM estimator is a suboptimal hybrid filter that was shown to achieve an excellent compromise between performance and complexity[REF]. In the IMM, each state estimate is computed under each possible current model using r filters, with each filter using a different combination of the previous model-conditioned estimates which are the mixed initial conditions. The regime switching is usually modeled by a finite state homogeneous Markov chain, with a priori known transition probabilities. As depicted in Figure 2, this algorithm can be divided into five stages: (1) calculation of mixing probabilities, (2) mixed initial states and covariances, (3) filtering, (4) mode probability update and (5) state estimate combination (output only,

stage five is not part of the recursion). The Transition Matrix of the Markov Chain M_{ij} - used on the mode probability update - is assumed constant over time (homogeneous).

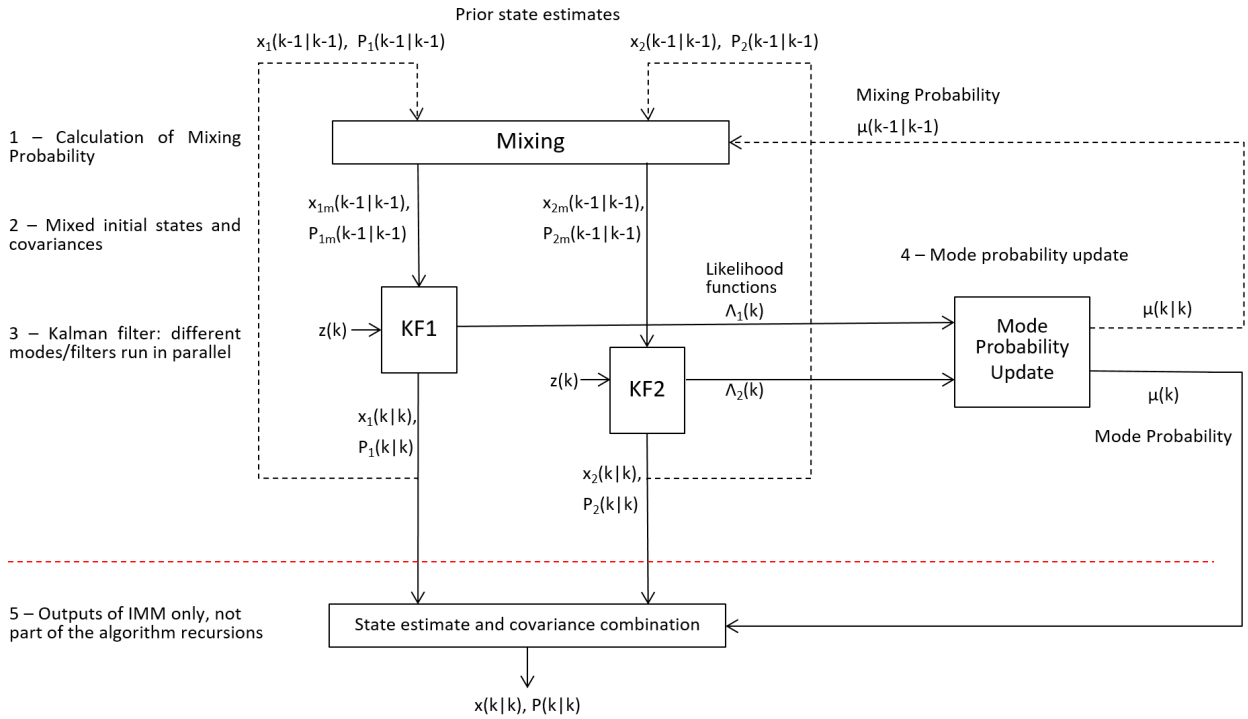

Figure 2: IMM Algorithm

II. Problem Formulation

II.A. Kalman Filters

Each state space model can be expressed with equations of the following form:

$$x_k = F_{k-1}x_{k-1} + G_{k-1}u_{k-1} + q_{k-1} \tag{1}$$

$$z_k = H_k x_k + r_k \tag{2}$$

where:

- $x_k \in R^n$ are the system states (intruder cartesian position, velocity, and acceleration in inertial coordinates) on time step k.
- F_{k-1} is the transition matrix of the dynamic model.
- G_{k-1} is the transition matrix of the dynamics of the own aircraft.
- u_{k-1} are the own aircraft states in inertial coordinates.
- $q_{k-1} \sim N(0; Q_{k-1})$ is the process noise on time step $k-1$.
- $z_k \in R^m$ is the cartesian relative intruder measurement on time step k.
- H_k is the measurement model matrix.
- $r_k \sim N(0; R_k)$ is the measurement noise on time step k.
- The initial distribution for the state is $x_0 \sim N(0; \hat{P}_0)$, where $\hat{P}_0$ is set to large values based on the lack of knowledge about our target.

The Kalman Filter has two steps: the prediction step, where the next state of the system is predicted given the previous measurements, and the update step, where the current state of the system is estimated given the measurement at that time step. The equation for these steps are as follows:[7]

Prediction:

$$\bar{x}_k = F_{k-1}\hat{x}_{k-1} + G_{k-1}u_{k-1} \tag{3}$$

$$\bar{P}_k = F_{k-1}\hat{P}_{k-1}F_{k-1}^T + Q_{k-1} \tag{4}$$

Update:

$$S_k = H_k\bar{P}_kH_k^T + R_k \tag{5}$$

$$K_k = \bar{P}_kH_k^TS_k^{-1} \tag{6}$$

$$\hat{x}_k = \bar{x}_k + K_k(z_k - H_k\bar{x}) \tag{7}$$

$$\hat{P}_k = \bar{P}_k - K_kS_kK_k^T; \tag{8}$$

Differently than most fixed radar applications (ATC as an example) in which the tracker is static, our DAA system will contain tracking sensors mounted on our unmanned aircraft. In this way, standard maneuvers such as a coordinated turn (CT) are viewed differently from the aircraft relative frame. We have to consider the transition from these reference frames in the formulation.

The inertial to relative frame transition matrix:

$$x_{k+1}^{rel} = x_{k+1}^I - x_{k+1}^O \tag{9}$$

$$x_{k+1}^I - x_{k+1}^O = F_k^Ix_k^I - F_k^Ox_k^O \tag{10}$$

$$x_{k+1}^I - x_{k+1}^O = F_k^Ix_k^I - F_k^Ox_k^O - F_k^Ix_k^O + F_k^Ix_k^O \tag{11}$$

$$x_{k+1}^{rel} = F_k^Ix_k^{rel} + [F^I - F^O]x_k^O \tag{12}$$

$$x_{k+1}^{rel} = F_k^Ix_k^{rel} + G_ku_k \tag{13}$$

where:

- x^{rel} is the state vector of the intruder aircraft in the own aircraft-centered relative frame.
- x^I is the state vector of the intruder aircraft on the inertial frame
- x^O is the state vector of the own aircraft on the inertial frame
- F^I is the state transition matrix of the intruder aircraft
- F^O is the state transition matrix of the own aircraft

In this way, we can use $[F^I - F^O] = G_k$ and $x_k^O = u_k$ as our input velocity from our own aircraft to correct the maneuvers to the relative frame. Our final Equation (13) is analogous to the Kalman Filter Equation (3).

II.B. Encounter Model

The MIT Lincoln Lab Encounter Model is based on radar data collected across the U.S.[8] The model is based on the use of dynamic variables to construct random aircraft trajectories that are statistically similar to those observed in the radar data. It only gives as an output the initial conditions and control variables for each time step. After initializing our simulated trajectory with the initial conditions, we are only interested in assigning new values based on the dynamic variables generated (linear acceleration $\dot{v}$, turn rate $\dot{\psi}$, and the vertical velocity $\dot{z}$).

II.C. Simulation Modes

Based on the potential ways the encounter model can build an intruder trajectory, we hypothesized requiring models for straight level flight, turns, linear acceleration, and climb/descent. This results in six modes, three different modes for 2D movement and the same three modes in 3D with the addition of the vertical velocity $\dot{z}$ to account for climb/descent:

- Mode 1 - Constant Velocity
- Mode 2 - Constant Velocity 3D (non-zero $\dot{z}$)
- Mode 3 - Coordinated Turn
- Mode 4 - Coordinated Turn 3D (non-zero $\dot{z}$)
- Mode 5 - Constant Linear Acceleration
- Mode 6 - Constant Linear Acceleration 3D (non-zero $\dot{z}$)

Modes 1 and 2 have six states:

$$X = \begin{bmatrix} x & \dot{x} & y & \dot{y} & z & \dot{z} \end{bmatrix}^T \tag{14}$$

Modes 3 through 6 have nine states:

$$X = \begin{bmatrix} x & \dot{x} & \ddot{x} & y & \dot{y} & \ddot{y} & z & \dot{z} & \ddot{z} \end{bmatrix}^T \tag{15}$$

The implementations of the Constant Velocity (CV) and Constant Acceleration (CA) filters are relatively straightforward. For the kinematic constraints CT model (modes 3 and 4), the state transition matrix is defined to perform a constant-speed turn along the trajectory which is defined by the state estimates of velocity and acceleration. The turning rate ω is defined by:

$$\omega = \frac{\|\mathbf{a}\|}{\|\mathbf{v}\|} = \frac{\sqrt{\ddot{x}^2 + \ddot{y}^2 + \ddot{z}^2}}{\sqrt{\dot{x}^2 + \dot{y}^2 + \dot{z}^2}} \tag{16}$$

where $\mathbf{a}$ and $\mathbf{v}$ are the accelerations and velocity vectors. Then, the transition matrices are based on the dynamics for the intruder F^I and own aircraft F^O are:

$$F^I = \begin{bmatrix} 1 & \frac{\sin(\omega T)}{\omega} & \frac{(1-\cos(\omega T))}{(\omega^2)} & 0 & 0 & 0 & 0 & 0 & 0 \\ 0 & \cos(\omega T) & \frac{\sin(\omega T)}{\omega} & 0 & 0 & 0 & 0 & 0 & 0 \\ 0 & -\omega\sin(\omega T) & \cos(\omega T) & 0 & 0 & 0 & 0 & 0 & 0 \\ 0 & 0 & 0 & 1 & \frac{\sin(\omega T)}{\omega} & \frac{(1-\cos(\omega T))}{(\omega^2)} & 0 & 0 & 0 \\ 0 & 0 & 0 & 0 & \cos(\omega T) & \frac{\sin(\omega T)}{\omega} & 0 & 0 & 0 \\ 0 & 0 & 0 & 0 & -\omega\sin(\omega T) & \cos(\omega T) & 0 & 0 & 0 \\ 0 & 0 & 0 & 0 & 0 & 0 & 1 & T & 0 \\ 0 & 0 & 0 & 0 & 0 & 0 & 0 & 1 & 0 \\ 0 & 0 & 0 & 0 & 0 & 0 & 0 & 0 & 0 \end{bmatrix} \tag{17}$$

$$F^O = \begin{bmatrix} 0 & T & 0 & 0 & 0 & 0 & 0 & 0 & 0 \\ 0 & 1 & 0 & 0 & 0 & 0 & 0 & 0 & 0 \\ 0 & 0 & 0 & 0 & 0 & 0 & 0 & 0 & 0 \\ 0 & 0 & 0 & 0 & T & 0 & 0 & 0 & 0 \\ 0 & 0 & 0 & 0 & 1 & 0 & 0 & 0 & 0 \\ 0 & 0 & 0 & 0 & 0 & 0 & 0 & 0 & 0 \\ 0 & 0 & 0 & 0 & 0 & 0 & 0 & T & 0 \\ 0 & 0 & 0 & 0 & 0 & 0 & 0 & 1 & 0 \\ 0 & 0 & 0 & 0 & 0 & 0 & 0 & 0 & 0 \end{bmatrix} \tag{18}$$

$$G = F^I - F^O = \begin{bmatrix} 1 & \frac{\sin(\omega T)}{\omega} - T & \frac{(1-\cos(\omega T))}{(\omega^2)} & 0 & 0 & 0 & 0 & 0 & 0 \\ 0 & \cos(\omega T) - 1 & \frac{\sin(\omega T)}{\omega} & 0 & 0 & 0 & 0 & 0 & 0 \\ 0 & -\omega \sin(\omega T) & \cos(\omega T) & 0 & 0 & 0 & 0 & 0 & 0 \\ 0 & 0 & 0 & 1 & \frac{\sin(\omega T)}{\omega} - T & \frac{(1-\cos(\omega T))}{(\omega^2)} & 0 & 0 & 0 \\ 0 & 0 & 0 & 0 & \cos(\omega T) - 1 & \frac{\sin(\omega T)}{\omega} & 0 & 0 & 0 \\ 0 & 0 & 0 & 0 & -\omega \sin(\omega T) & \cos(\omega T) & 0 & 0 & 0 \\ 0 & 0 & 0 & 0 & 0 & 0 & 1 & 0 & 0 \\ 0 & 0 & 0 & 0 & 0 & 0 & 0 & 0 & 0 \\ 0 & 0 & 0 & 0 & 0 & 0 & 0 & 0 & 0 \end{bmatrix} \tag{19}$$

where T is the simulation timestep.

$$\mathbf{u} = \begin{bmatrix} 0 & \dot{x}_{own} & 0 & 0 & \dot{y}_{own} & 0 & 0 & \dot{z}_{own} & 0 \end{bmatrix}^T \tag{20}$$

where $\dot{x}_{own}$, $\dot{y}_{own}$ and $\dot{z}_{own}$ are the own aircraft velocity components.

Considering that we have only position measurements, the measurement matrix is:

$$H = \begin{bmatrix} 1 & 0 & 0 & 0 & 0 & 0 & 0 & 0 & 0 \\ 0 & 0 & 0 & 1 & 0 & 0 & 0 & 0 & 0 \\ 0 & 0 & 0 & 0 & 0 & 0 & 1 & 0 & 0 \end{bmatrix} \tag{21}$$

The matrices for the other modes can be found in the Appendix.

II.D. Determination of the Transition Probabilities for the IMM

The results of IMM algorithm simulations, cited in many papers, show a good performance of this algorithm in terms of track confirmation and maintenance. In this estimation, the Transition Matrix of the Markov Chain is almost always assumed to be known. A new generation of MM estimators assumes that the Transition Matrix of the Markov Chain governing the mode jumps is known. However, it is very difficult to determine the appropriate matrix quantities and identify a Markov transition law that optimally fits the unknown target motion.[9]

Fortunately, we can use the encounter model to better account for the real likelihood of the mode switching based on these radar observations.[8] We ran the Encounter Model, described in Section II.B., 10^6 times and recorded each mode transition. We used these runs to build the Transition Matrix, outlined in Equation (24) in the Appendix.

II.E. Simulation Steps

First we generate and extract the initial conditions and control variables from Encounter Model. These are only scalars (velocity, linear acceleration, turn rate, and the vertical velocity) so we need to provide a initial position and direction in relation to our own aircraft. We initialize the position of the intruder aircraft on the surface of the encounter cylinder centered on the own aircraft, at a random heading angle. The probability of being initialized on the on the top, bottom, or side surfaces of the encounter cylinder is proportional to the surface area of each. For this analysis, the encounter cylinder is assumed to have a ±3000ft height and 5NM radius.[10] We apply sampling rejection for the initial position conjugated with the initial conditions from the Encounter Model. If the intruder is not in an inward trajectory from the surface, we repeat the initialization.

Since the trajectory construction is not provided in the encounter model, we build the trajectory using point-mass kinematics to update the aircraft states. The trajectory is then inserted into the IMM estimation algorithm, using the Encounter Model outputs as inputs for the true intruder trajectory. Finally, we get the

simulation outputs for analysis as shown in Figure 3.

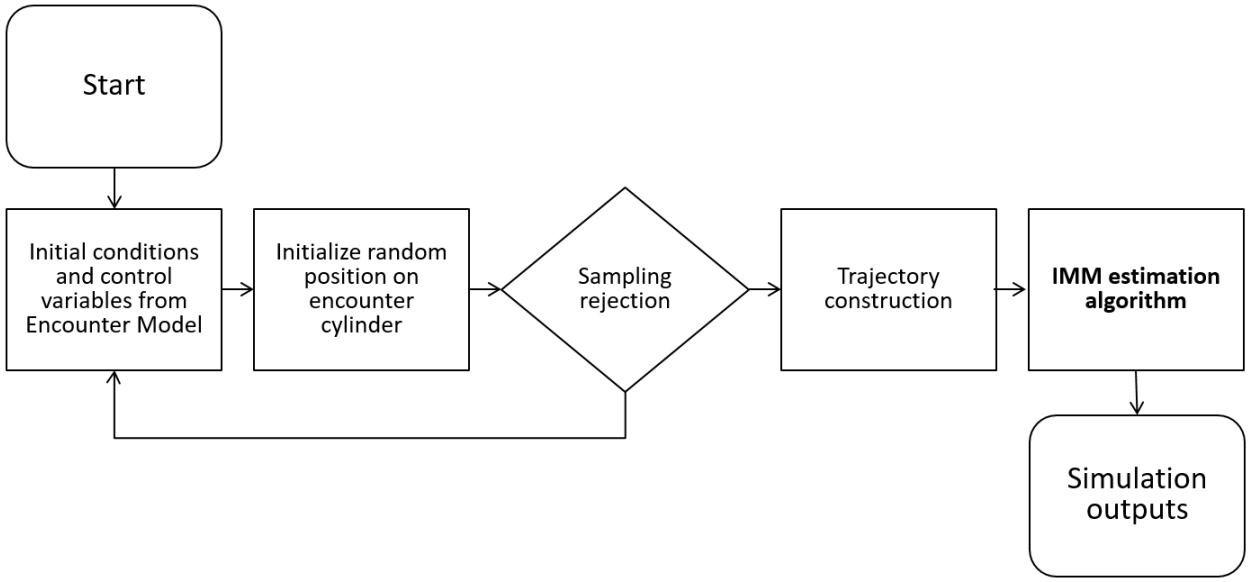

Figure 3: Simulation Structure

III. Error Analysis

The IMM algorithm has estimation errors that are not directly related with its calculated covariances. In this way, the total error in the states , CPA, and trajectory prediction will be a sum of different error sources. Some will depend on the quality of the implementation of the algorithm, others on the inherently noisy measurements from the DAA system. In summary, we can divide the main contributors of the error in:

- KF modeling error: This is partly due to the modeling errors, where a maneuver, by its nature, does not follow the assumptions of the standard maneuvers on the Kalman Filters used in the IMM.[11]
- Sensor noise: Random noise on the sensors measurements.
- Mode prediction: A relatively large estimation error is needed for the algorithm to recognize sudden changes in system modes, i.e. the adaptation might not be rapid enough. We will introduce later the Perfect IMM, in which the true mode of the target is known, for performance comparison.

In a real IMM, even with perfect measurements, we would still have uncertainty in trajectory estimation due to the approximate motion models used.

III.A. Perfect IMM (PIMM

In these simulations, the true motion of the target is known. For this simulation, the output from the intruder is defined by the encounter model, and the PIMM switches to the correct motion model at each mode change. Since the Perfect IMM always selects the right motion model, it defines the lower bound on the IMM estimation error for any given sensor error model. In our DAA sensor analysis, the importance of this lower bound is that we know that we cannot improve the state estimation on the IMM beyond the Perfect IMM results, given the same modes and conditions.

III.B. CPA prediction

The DAA MOPS describes the hazard associated with a UAS failing to self-separate. The hazard states are the variables that define the well clear threshold (WCT), which are synonymous with the loss of DAA Well

Clear. Based on the DAA MOPS, these variables are: Modified Tau (or Modified Time to Horizontal Closest Point of Approach), Horizontal Closest Point of Approach (CPA), and Predicted Vertical Separation.

Since we are interested in the effects on turning trajectories, when compared to previous work done on linear trajectories, we focus this paper on the effects of the IMM estimation on CPA. We leave the analysis on Modified Tau and Vertical Separation for future work. Then we can use the CPA prediction error as a benchmark for our algorithm performance and analysis.

There are two ways to determine the Horizontal CPA, r_{CPA}. One is the time based definition in the DAA MOPS and the other is geometrically determined based on a linear intruder trajectory. The geometric r_{CPA} can be derived from the definition[12] and its expression is:

$$r_{CPA} = \frac{\dot{y}x - \dot{x}y}{\sqrt{\dot{x}^2 + \dot{y}^2}} \tag{22}$$

IV. Simulation and Discussion

The analysis was done, following the flowchart in Figure 3. For all the different encounters simulated, the own aircraft was assumed to have linear trajectory, with constant velocity of 200kt, while the generated trajectory for the intruder aircraft is randomly generated by the encounter model. Each of the trajectories are simulated for 50 seconds of total simulation time, with a sample rate of 1 Hz.

IV.A. Experiment Setup

We are interested in isolating the residual error due to our modeling. With zero measurement noise, and comparing with the Perfect IMM, we are looking at how suitable our model is to deal with the eventual maneuvers without knowledge of the true intruder aircraft dynamics. For performance comparisons, we are running the IMM and PIMM algorithms against the isolated Kalman Filters that correspond to each different mode, outside of the IMM algorithm context, i.e. with no mixed initial conditions. The mixed initial conditions are already an improvement due to the IMM algorithm and should not be used on the pure Kalman Filters.

IV.B. Results

Example of one particular trajectory

Running one particular trajectory, we can observe what are the outputs from the simulation as well as the general behavior of mode switching and how long the adaptation to a new mode takes. Most of the trajectories generated will be constant velocity straight level flight due to their higher likelihood. Since we are interested in testing the adaptation to mode changes and see the performance of the algorithm in more extreme cases, we picked a trajectory with non-zero values for the three control variables generated from the encounter model, as shown in Figure 4.

The trajectory shows the intruder aircraft coming from behind the own aircraft, generated at the top surface of the encounter cylinder, accelerating, performing a turn and descending during different parts of the trajectory, as shown in Figure 5. The cylinders shown are the encounter cylinder ($\pm$3000ft height, 5NM radius) and the WCT ($\pm$450 ft height, 4000 ft radius)

In Figure 6, we can observe the different behavior on the mode probabilities of the IMM and the Perfect IMM algorithms. As expected, the PIMM switches instantaneously to new mode as the control variables changes. It is also observed the soft switching that occurs along a few time-steps once the algorithm recognizes a new mode.

In Figure 7, we can see that the IMM and the Perfect IMM performance on the CPA estimation error are quite similar. The main difference was the adaptation time or lag after a maneuver change and the algorithm detection. After this, both slowly tend to zero as the models gets better prediction on the states with time.

Monte Carlo simulation

Even with the trajectory rejection sampling as detailed in Figure 3, we still have numerous trajectories that are not very interesting, going out of the cylinder after a few timesteps or just straight level flights

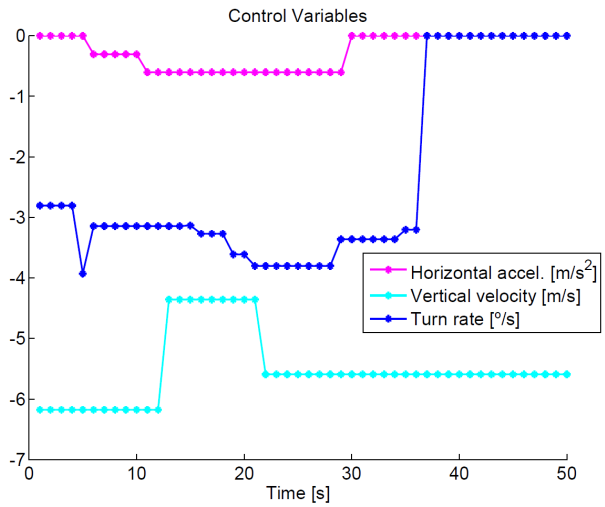

Figure 4: Control variables used on the simulation

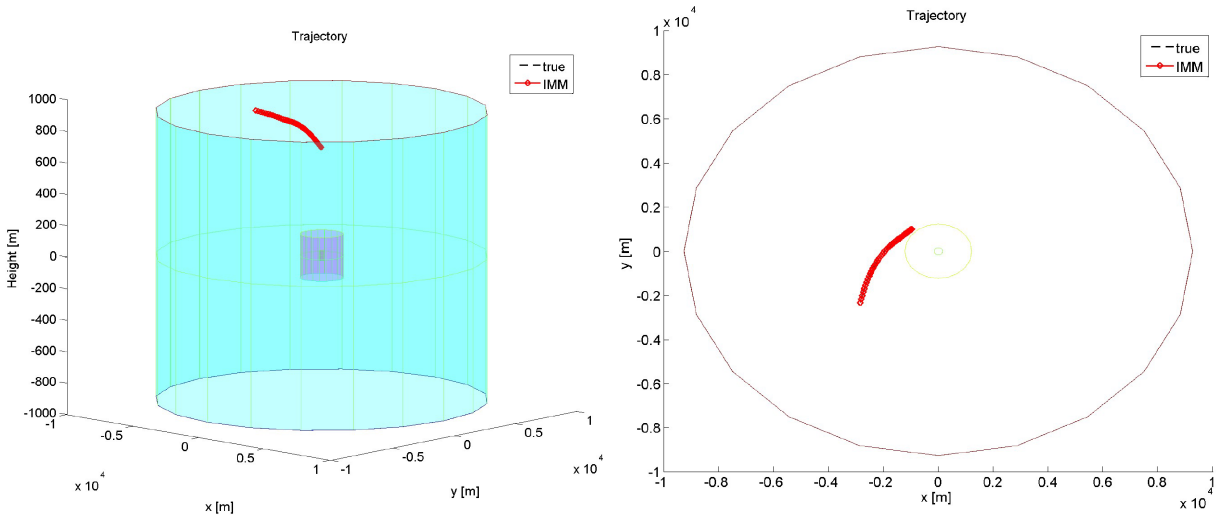

Figure 5: Trajectory of the simulation

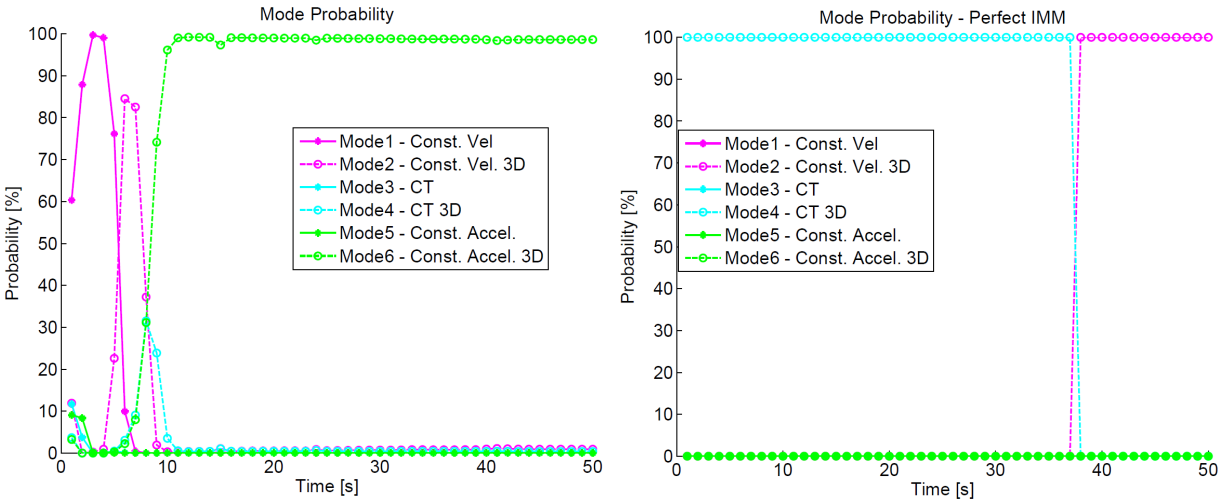

Figure 6: Mode probability comparison

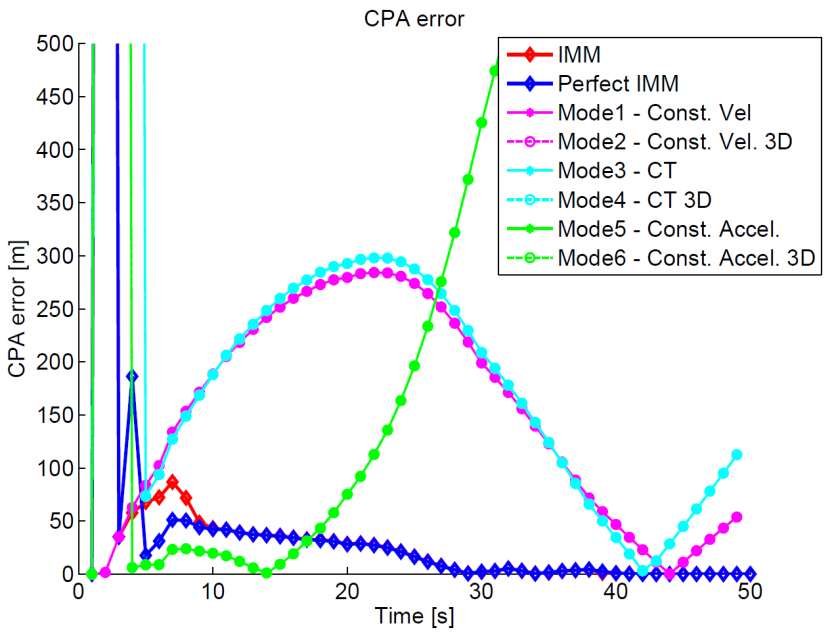

Figure 7: CPA error estimation

that impose no danger to the WCT. In this way, for this particular analysis we are interested only in the trajectories for where the $r_{CPA} < WCT$.

To analyze the the general performance of the IMM compared with normal Kalman Filters, we run 10^5 simulations and calculate $RMS(CPAerror)$ for each one of the filters. Since each of the KF or IMM modes takes some timesteps to stabilize, we calculate the RMS values of the CPA error starting at different timesteps T_s to account for the adaptation time. Calculating the mean value of the RMS of the CPA estimation error gives us the following Table 1:

	$T_s = 5s$	$T_s = 10s$	$T_s = 15s$	$T_s = 20s$
Mode1	471.2	402.0	394.7	399.6
Mode2	471.2	402.0	394.7	399.6
Mode3	711.6	735.1	743.6	757.1
Mode4	712.7	734.3	743.2	756.4
Mode5	1377.6	1233.3	1147.6	1081.3
Mode6	1377.6	1233.3	1147.6	1081.3
IMM	50.5	34.3	32.8	31.5
PIMM	66.3	34.0	32.6	31.3

Table 1: Mean RMS of CPA error estimation of 10^5 trajectories

IV.C. Adding more modes

Our initial hypothesis was to define a different mode for each of the possible combination from the outcomes for the outputs for the Encounter Model in its control variables. For the combination of the 3 different control variables, we would have 8 different modes considering that each can be zero or non-zero. For the coordinated turn with fixed turn rate, we would need to split in positive and negative turn rates, driving the total number of modes to 10. The following potential filters were considered, including two different types of CT filters:

- Constant Velocity 2D

- Coordinated Turn (fixed turn rate +) 2D
- Coordinated Turn (fixed turn rate -) 2D
- Constant Velocity 3D
- Constant Linear Acceleration 2D
- Coordinated Turn (fixed turn rate +) 3D
- Coordinated Turn (fixed turn rate -) 3D
- Coordinated Turn (kinematics constraint model) 2D
- Constant Linear Acceleration 3D
- Coordinated Turn (kinematics constraint model) 3D

As can be seen in Figure 9 on the green and yellow modes, the performance of the fixed turn rate Coordinated Turn model were poor compared to the others. Even after an analysis using the data from the Encounter Model to find the most likely value for the turn (which was about 3.5 degrees, close the standard turn rate, as shown in Figure 8), the better performance of the other CT model drives the IMM to give more weighting to the later. Since the use of the fixed CT model did not improved the estimation, we dropped this in favor of the kinematics constraints CT model only.

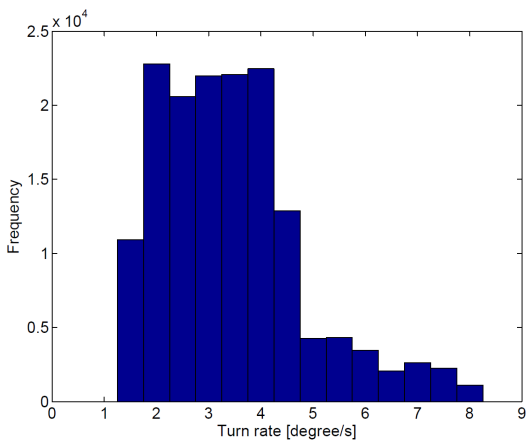

Figure 8: Histogram of the turn rates distribution over 10^6 timesteps

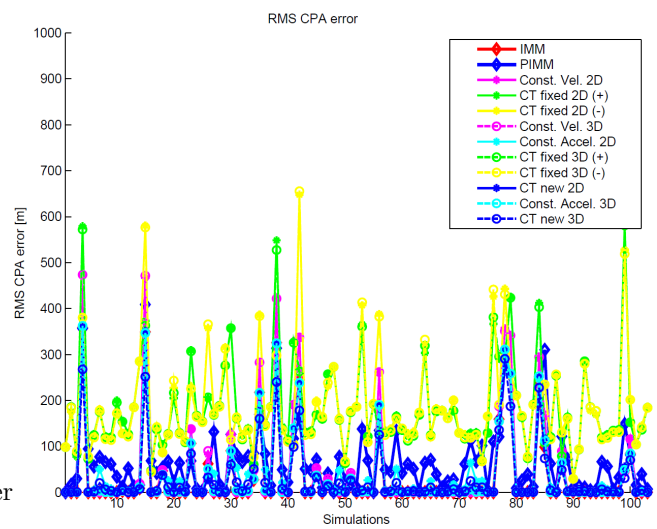

Figure 9: Performance comparison of the filters

IV.D. Summary

We ran certain encounter model trajectories and did a RMS analysis comparing the IMM and PIMM performance to the individual filters. The IMM and PIMM showed a reduction in the CPA error estimation under the random trajectories. It was showed that adding a dedicated CT filter with fixed turn rate didn't work as well as the original six modes on the previous analysis.

V. Conclusion

From the results shown, the CPA estimation error is considerably reduced by the use of the IMM algorithm. For the modes used, the difference between the performance of the IMM and the Perfect IMM was negligible when considering the RMS error. The main difference consisted in the adaptation time or lag between a maneuver change and the algorithm detection, although this was a few seconds, for most of the trajectories.

One of the limitations is that since we can not predict an intruder aircraft maneuver (i.e. mode changes), even for the Perfect IMM we are using estimations that depend on the mode adaptation to the new trajectory. The magnitude of the error in the CPA estimation will depend on when the change happens at the trajectory, the geometry of the encounter, and the magnitude of the change in the trajectory, a high turn rate change when the previous state was constant velocity as an example. And in this example, it will be dependent on the quality of the turn rate estimation by the CT filter and how long it takes to stabilize.

The importance of a good estimation and trajectory prediction under maneuver is also evidenced by the high CPA error for the regular Kalman Filters under maneuver changes including turns. This is due to the sensitivity in the CPA prediction with the direction of the velocity vector. The residual error is highly dependent on the model switching and the geometry of the trajectory, even for perfect measurements and for our Perfect IMM model.

Adding more modes does not necessarily improve the results on the IMM performance. For example, the fixed Coordinated Turn mode did not presented good results for trajectories out of the their fixed turn rate range, when compared to the kinematics contraints model.

The algorithms employed inside this DAA sensor context, utilizing realistic encounter model generated trajectories seems promising considering the residual error reduction from the Kalman Filters used for the individual modes. Further work on this area should include realistic modeling for the sensor error to fully account the error sources as well as analysis of the impact of the IMM on the other hazard states (Tau and Vertical Separation).

Appendix

Transition Matrix and Probability Vector (6 modes)

Initial mode probabilities:

$$\boldsymbol{\mu_{ip}} = \begin{bmatrix} 0.55117 & 0.15393 & 0.10708 & 0.04781 & 0.09292 & 0.04709 \end{bmatrix} \tag{23}$$

Transition Matrix of the Markov Chain:

$$M_{ij} = \begin{bmatrix} 0.98038 & 0.00692 & 0.00562 & 0.00093 & 0.00508 & 0.00108 \\ 0.02536 & 0.96022 & 0.00246 & 0.00509 & 0.00200 & 0.00487 \\ 0.03263 & 0.00280 & 0.95063 & 0.00646 & 0.00624 & 0.00123 \\ 0.01280 & 0.01891 & 0.01456 & 0.94566 & 0.00172 & 0.00636 \\ 0.02551 & 0.00250 & 0.01098 & 0.00077 & 0.95314 & 0.00710 \\ 0.00926 & 0.01860 & 0.00204 & 0.01147 & 0.01049 & 0.94814 \end{bmatrix} \tag{24}$$

Transition Matrices of the Modes

For Modes 1-2:

$$\mathbf{x} = \begin{bmatrix} x & \dot{x} & y & \dot{y} & z & \dot{z} \end{bmatrix}^T \tag{25}$$

$$F^O = \begin{bmatrix} 0 & T & 0 & 0 & 0 & 0 \\ 0 & 1 & 0 & 0 & 0 & 0 \\ 0 & 0 & 0 & T & 0 & 0 \\ 0 & 0 & 0 & 1 & 0 & 0 \\ 0 & 0 & 0 & 0 & 0 & T \\ 0 & 0 & 0 & 0 & 0 & 1 \end{bmatrix} \tag{26}$$

$$G = F^I - F^O \tag{27}$$

$$\mathbf{u} = \begin{bmatrix} 0 & \dot{x}_{own} & 0 & \dot{y}_{own} & 0 & \dot{z}_{own} \end{bmatrix}^T \tag{28}$$

$$H = \begin{bmatrix} 1 & 0 & 0 & 0 & 0 & 0 \\ 0 & 0 & 1 & 0 & 0 & 0 \\ 0 & 0 & 0 & 0 & 1 & 0 \end{bmatrix} \tag{29}$$

For Modes 3-6:

$$\mathbf{x} = \begin{bmatrix} x & \dot{x} & \ddot{x} & y & \dot{y} & \ddot{y} & z & \dot{z} & \ddot{z} \end{bmatrix}^T \tag{30}$$

$$F^O = \begin{bmatrix} 0 & T & 0 & 0 & 0 & 0 & 0 & 0 & 0 \\ 0 & 1 & 0 & 0 & 0 & 0 & 0 & 0 & 0 \\ 0 & 0 & 0 & 0 & 0 & 0 & 0 & 0 & 0 \\ 0 & 0 & 0 & 0 & T & 0 & 0 & 0 & 0 \\ 0 & 0 & 0 & 0 & 1 & 0 & 0 & 0 & 0 \\ 0 & 0 & 0 & 0 & 0 & 0 & 0 & 0 & 0 \\ 0 & 0 & 0 & 0 & 0 & 0 & 0 & T & 0 \\ 0 & 0 & 0 & 0 & 0 & 0 & 0 & 1 & 0 \\ 0 & 0 & 0 & 0 & 0 & 0 & 0 & 0 & 0 \end{bmatrix} \tag{31}$$

$$G = F^I - F^O \tag{32}$$

$$\mathbf{u} = \begin{bmatrix} 0 & \dot{x}_{own} & 0 & 0 & \dot{y}_{own} & 0 & 0 & \dot{z}_{own} & 0 \end{bmatrix}^T \tag{33}$$

$$H = \begin{bmatrix} 1 & 0 & 0 & 0 & 0 & 0 & 0 & 0 & 0 \\ 0 & 0 & 0 & 1 & 0 & 0 & 0 & 0 & 0 \\ 0 & 0 & 0 & 0 & 0 & 0 & 1 & 0 & 0 \end{bmatrix} \tag{34}$$

- Mode 1 - Constant velocity

$$F^I = \begin{bmatrix} 1 & T & 0 & 0 & 0 & 0 \\ 0 & 1 & 0 & 0 & 0 & 0 \\ 0 & 0 & 1 & T & 0 & 0 \\ 0 & 0 & 0 & 1 & 0 & 0 \\ 0 & 0 & 0 & 0 & 1 & 0 \\ 0 & 0 & 0 & 0 & 0 & 0 \end{bmatrix} \tag{35}$$

- Mode 2 - Constant velocity 3D

$$F^I = \begin{bmatrix} 1 & T & 0 & 0 & 0 & 0 \\ 0 & 1 & 0 & 0 & 0 & 0 \\ 0 & 0 & 1 & T & 0 & 0 \\ 0 & 0 & 0 & 1 & 0 & 0 \\ 0 & 0 & 0 & 0 & 1 & T \\ 0 & 0 & 0 & 0 & 0 & 1 \end{bmatrix} \tag{36}$$

- Mode 3 - Coordinated Turn Model (kinematics constraints)

$$F^I = \begin{bmatrix} 1 & \frac{\sin(\omega T)}{\omega} & \frac{1-\cos(\omega T)}{\omega^2} & 0 & 0 & 0 & 0 & 0 & 0 \\ 0 & \cos(\omega T) & \frac{\sin(\omega T)}{\omega} & 0 & 0 & 0 & 0 & 0 & 0 \\ 0 & -\omega\sin(\omega T) & \cos(\omega T) & 0 & 0 & 0 & 0 & 0 & 0 \\ 0 & 0 & 0 & 1 & \frac{\sin(\omega T)}{\omega} & \frac{1-\cos(\omega T)}{\omega^2} & 0 & 0 & 0 \\ 0 & 0 & 0 & 0 & \cos(\omega T) & \frac{\sin(\omega T)}{\omega} & 0 & 0 & 0 \\ 0 & 0 & 0 & 0 & -\omega\sin(\omega T) & \cos(\omega T) & 0 & 0 & 0 \\ 0 & 0 & 0 & 0 & 0 & 0 & 1 & 0 & 0 \\ 0 & 0 & 0 & 0 & 0 & 0 & 0 & 0 & 0 \\ 0 & 0 & 0 & 0 & 0 & 0 & 0 & 0 & 0 \end{bmatrix} \tag{37}$$

- Mode 4 - Coordinated Turn Model (kinematics constraints) - 3D

$$F^I = \begin{bmatrix} 1 & \frac{\sin(\omega T)}{\omega} & \frac{1-\cos(\omega T)}{\omega^2} & 0 & 0 & 0 & 0 & 0 & 0 \\ 0 & \cos(\omega T) & \frac{\sin(\omega T)}{\omega} & 0 & 0 & 0 & 0 & 0 & 0 \\ 0 & -\omega\sin(\omega T) & \cos(\omega T) & 0 & 0 & 0 & 0 & 0 & 0 \\ 0 & 0 & 0 & 1 & \frac{\sin(\omega T)}{\omega} & \frac{1-\cos(\omega T)}{\omega^2} & 0 & 0 & 0 \\ 0 & 0 & 0 & 0 & \cos(\omega T) & \frac{\sin(\omega T)}{\omega} & 0 & 0 & 0 \\ 0 & 0 & 0 & 0 & -\omega\sin(\omega T) & \cos(\omega T) & 0 & 0 & 0 \\ 0 & 0 & 0 & 0 & 0 & 0 & 1 & T & 0 \\ 0 & 0 & 0 & 0 & 0 & 0 & 0 & 1 & 0 \\ 0 & 0 & 0 & 0 & 0 & 0 & 0 & 0 & 0 \end{bmatrix} \tag{38}$$

- Mode 5 - Constant Linear Acceleration

$$F^I = \begin{bmatrix} 1 & T & T^2/2 & 0 & 0 & 0 & 0 & 0 & 0 \\ 0 & 1 & T & 0 & 0 & 0 & 0 & 0 & 0 \\ 0 & 0 & 1 & 0 & 0 & 0 & 0 & 0 & 0 \\ 0 & 0 & 0 & 1 & T & T^2/2 & 0 & 0 & 0 \\ 0 & 0 & 0 & 0 & 1 & T & 0 & 0 & 0 \\ 0 & 0 & 0 & 0 & 0 & 1 & 0 & 0 & 0 \\ 0 & 0 & 0 & 0 & 0 & 0 & 1 & 0 & 0 \\ 0 & 0 & 0 & 0 & 0 & 0 & 0 & 0 & 0 \\ 0 & 0 & 0 & 0 & 0 & 0 & 0 & 0 & 0 \end{bmatrix} \tag{39}$$

- Mode 6 - Constant Linear Acceleration - 3D

$$F^I = \begin{bmatrix} 1 & T & T^2/2 & 0 & 0 & 0 & 0 & 0 & 0 \\ 0 & 1 & T & 0 & 0 & 0 & 0 & 0 & 0 \\ 0 & 0 & 1 & 0 & 0 & 0 & 0 & 0 & 0 \\ 0 & 0 & 0 & 1 & T & T^2/2 & 0 & 0 & 0 \\ 0 & 0 & 0 & 0 & 1 & T & 0 & 0 & 0 \\ 0 & 0 & 0 & 0 & 0 & 1 & 0 & 0 & 0 \\ 0 & 0 & 0 & 0 & 0 & 0 & 1 & T & 0 \\ 0 & 0 & 0 & 0 & 0 & 0 & 0 & 1 & 0 \\ 0 & 0 & 0 & 0 & 0 & 0 & 0 & 0 & 0 \end{bmatrix} \tag{40}$$

Acknowledgments

This work is supported by the Brazilian agency Capes through a scholarship from Ciencia sem Fronteiras (Science without Borders) program / Processo No. 99999.012923/2013-03.

References

[1]RTCA SC-159, "Minimum Aviation System Performance Standards for the Local Area Augmentation System," 2004.

[2]Yu, X. and Zhang, Y., "Sense and avoid technologies with applications to unmanned aircraft systems: Review and prospects," *Progress in Aerospace Sciences*, Vol. 74, Apr 2015, pp. 152–166.

[3]Zeitlin, A. D., "Sense & Avoid Capability Development Challenges," *IEEE Aerospace and Electronic Systems Magazine*, Vol. 25, No. 10, Oct 2010, pp. 27–32.

[4]Federal Aviation Administration, "Advisory Circular 25.1309-1A - System Design and Analysis," Jun 1988.

[5]RTCA SC-228, "Draft Detect and Avoid Minimum Operational Performance Standards for Verification and Validation," Sep 2015.

[6]Federal Aviation Administration, "Sense and Avoid (SAA) for Unmanned Aircraft Systems (UAS), SAA Workshop Second Caucus Report," Jan 2013.

[7]Bar-Shalom, Y., Kirubarajan, T., and Li, X.-R., *Estimation with applications to tracking and navigation:*, Wiley, 2007.

[8]Kochenderfer, M. J., Kuchar, J. K., Espindle, L. P., and Griffith, J. D., "Uncorrelated Encounter Model of the National Airspace System," Project Report ATC-345, Massachusetts Institute of Technology, Lincoln Laboratory, 2008.

[9]Radosavljevi, Z., "Determination of the Transition Probabilities for the Interacting Multiple Model Probabilistic Data Association Estimator," *Scientific Technical Review*, Vol. Vol.LVII, No. No.2, 2007, pp. 31–37.

[10]RTCA SC-228, "Draft Detect and Avoid Minimum Operational Performance Standards for Verification and Validation," Apr 2016.

[11]X. RONG LI, Y. B.-S., "Performance Prediction of the Interacting Multiple Model Algorithm," *IEEE Transactions On Aerospace And Electronic Systems*, Vol. VOL. 29, No. 3, jul 1993, pp. 775–771.

[12]JAMOOM, M. B., *UNMANNED AIRCRAFT SYSTEM SENSE AND AVOID INTEGRITY AND CONTINUITY*, Ph.D. thesis, Illinois Institute of Technology, may 2016.